Exterior Spacecraft Subsystem Protective Shielding Analysis and Design

William P. Schonberg*
University of Alabama in Huntsville, Huntsville, Alabama 35899
and
Roy A. Taylor†
NASA Marshall Space Flight Center, Huntsville, Alabama 35812

All spacecraft are susceptible to impacts by meteoroids and pieces of orbiting space debris. Such impacts are expected to occur at extremely high speeds and can damage internal and external flight-critical systems of spacecraft. An effective mechanism is developed to protect external spacecraft subsystems against damage by ricochet particles formed during such impacts. Equations and design procedures for protective shield panels are developed based on observed ricochet phenomena and calculated ricochet particle sizes and speeds. It is found that the diameter of the most damaging ricochet debris particle can be as large as 40% of the original project tile diameter and can travel at speeds between 24 and 36% of the original projectile impact velocity. Panel dimensions are shown to be strongly dependent on their inclination to the impact velocity vector and on their distribution around a spacecraft module. It is concluded that obliquity effects of high-speed impacts must be considered in the design of any structure exposed to the meteoroid and space debris environment.

Introduction

ALL spacecraft are susceptible to impacts by meteoroids and pieces of space debris. The more time spent in orbit, the more susceptible the spacecraft becomes to such impacts. These impacts are expected to occur at extremely high speeds and are expected to strike the spacecraft structure at oblique angles.[1] In a recent investigation of hypervelocity impact, it was demonstrated that oblique high-speed impacts generate a tremendous volume of ricochet debris, especially for impact trajectories above 45 deg.[2] It was observed that the damage potential of ricochet debris is very great and that the creation of such debris is a dangerous phenomenon that deserves further attention. Uncontained ricochet debris also increases the contamination of the orbital environment and can pose a threat to future missions into that environment.

The design of a spacecraft for a long-duration mission must address the possibility of space debris impacts and the effects of such impacts on the integrity of the entire spacecraft structure. Protective systems for habitable portions and for external structural subsytems must be included in its design. Protection against penetration for crew compartments and modules has traditionally consisted of a bumper plate that is placed a small distance away from the main pressure wall of the compartment or module. This concept was first proposed by Whipple[3] and has been studied extensively in the last two decades as a means of reducing the penetration threat of hypervelocity projectiles.[4-15] In the design process, bumper and pressure wall plate thicknesses are iterated against weight and protection considerations to arrive at a final configuration. However, protective measures for external spacecraft systems against ricochet debris impact damage have yet to be developed.

This paper presents the development of an efficient protection mechanism that will safeguard external spacecraft systems against ricochet debris impact damage and will also contain the spread of the ricochet debris particles. In the first section, a review of the experimental procedure used in the oblique hypervelocity impact testing of dual-wall specimens is presented. In the next section, the damage potential of ricochet debris is analyzed by determining the sizes and speeds of the most damaging ricochet debris particles. In subsequent sections, equations and design procedures for the external subsystem protection/debris-containment system are developed based on observed ricochet phenomena and predicted ricochet particle sizes and speeds. Several design examples are also presented and discussed.

Experimental Procedure and Results

The oblique hypervelocity impact testing of multisheet specimens was performed at the Space Debris Simulation Facility of the Materials and Processes Laboratory at the NASA Marshall Space Flight Center.[16] The facility consists of a light gas gun with a 12.7 mm launch tube capable of launching 2.5-12.7 mm projectiles of mass 4-300 mg at velocities of 2-8 km/s. Projectile velocity measurements were accomplished via pulsed x ray, laser diode detectors, and a Hall photographic station. A drawing of a typical dual-wall specimen setup is shown in Fig. 1.

In each test, a spherical projectile of diameter D and velocity V impacted a bumper plate of thickness t_s at an angle of obliquity θ. The projectile was shattered upon impact and created an elliptical hole in the bumper plate. Secondary projectile and bumper plate fragments were sprayed upon the pressure wall plate a distance S away while some fragments ricocheted and struck the ricochet witness plate. The angles θ_1 and θ_2 denote the trajectories of the centers of mass of bumper fragments and "in-line" penetration fragments, respectively; the angles γ_1 and γ_2 represent the spread of these fragments. The angles α_c and α_{99} characterize the trajectory of the center

Received Dec. 9, 1988; revision received Aug. 14, 1989. Copyright © 1989 American Institute of Aeronautics and Astronautics, Inc. No copyright is asserted in the United States under Title 17, U.S. Code. The U.S. Government has a royalty-free license to exercise all rights under the copyright claimed herein for Governmental purposes. All other rights are reserved by the copyright owner.

*Assistant Professor, Department of Mechanical Engineering. Member AIAA.

†Chief, Laboratory Support Branch, Materials and Processes Laboratory.

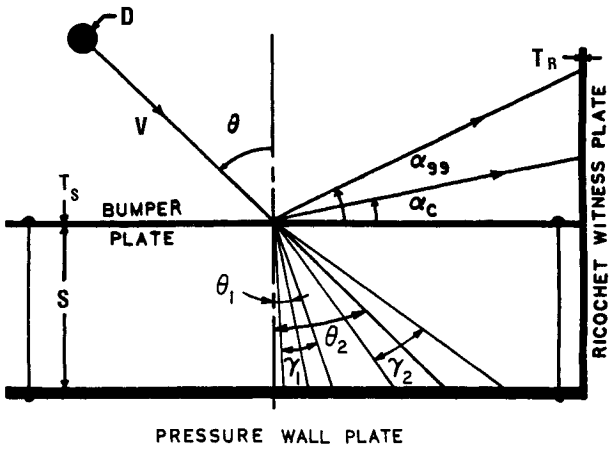

Fig. 1 Test specimen configuration and parameter definitions.

of mass of the ricochet fragment cloud and the angle below which lie 99% of the ricochet fragment trajectories, respectively. The formation and growth of penetration and ricochet debris clouds are clearly visible in high-speed photographs of the impact process.[17]

The conditions of the impact tests were chosen to simulate space debris impact of light-weight metallic space structures as closely as possible, and still remain within the realm of experimental feasibility. Kessler[18] states that the average mass density for pieces of orbital space debris less than 10 mm in diameter is approximately 2.8 g/cm^3, which is approximately the same as the density of aluminum. Although it is anticipated that the shape of the impacting projectile will affect the formation of penetration and ricochet debris, spherical projectiles were used in the test program to maintain repeatability and consistency. Thus, the projectiles were solid 1100 aluminum spheres with diameters ranging from 4.75 to 7.95 mm. The bumper, pressure wall, and ricochet witness plates were made of 6061-T6, 2219-T87, and 2219-T87 aluminum, respectively. The thicknesses of the bumper and pressure wall plates held constant at 1.625 and 3.175 mm, respectively, whereas those of the ricochet witness plates were varied from 2.54 to 25.4 mm. The bumper and pressure wall plates were separated by a constant distance of 101.6 mm. The obliquity of the impact was varied from 45 to 75 deg, and the impact velocities ranged from 6.7 to 8.0 km/s.

Ricochet Particle Size and Velocity Analysis

Damage potential estimates of ricochet debris particles created in an oblique hypervelocity impact will contribute significantly to the successful design of an effective protection mechanism for external spacecraft components. For the purposes of this investigation, the damage potential of a ricochet debris particle was assumed to be completely characterized by its size and speed. Equations for penetration depth and surface diameter of hypervelocity impact craters in thick plates were used together with measured depth and diameter values to calculate the diameter and velocity of a debris particle that caused a particular crater. Visual inspection of damaged ricochet witness plates reveal several interesting features that address the validity of this method.

1) The surface openings of ricochet witness plate craters formed by debris impacts were very nearly circular, which is indicative of near-normal impact trajectories. This observation is confirmed by oblique impact test data, which indicate that 99% of the ricochet debris impact obliquities are less than 30 deg, regardless of the original angle of impact.[19]

2) In the tests where the ricochet witness plates were sufficiently thick, the reverse sides of the plates remained smooth and undamaged even though the front sides exhibited significant crater damage. In these cases, the postimpact appearance of the ricochet witness plate was identical to that of a "thick plate" subjected to the same debris particle impact loading.

Based on these observations, the use of thick plate equations for penetration depth and crater diameter due to normal hypervelocity impact is justified provided that the reverse side of the ricochet witness plate in which the crater depths are measured is smooth and undamaged (ie., no spall or dimpling).

Examination of existing penetration depth equations revealed a strong coupling between particle size and velocity effects. That is, the same size crater can be produced by a small particle traveling at a high speed or by a larger particle traveling at a slower speed. Therefore, in order to have a unique solution for particle size and speed, a second set of equations describing another measurable crater quantity was needed. A search of existing literature on cratering phenomena in hypervelocity impact suggested crater volume to be such a quantity (Refs. 26, 28, 31, 33, 34, 36). Thus, a crater volume equation used in conjunction with an equation for penetration depth could be used to solve uniquely for particle size and speed. Since it is more facile to measure the surface diameter of an impact crater than it is to determine its exact volume, the crater volume equations were rewritten in terms of surface diameter. The analysis then proceeded as follows.

First, penetration depths and surface diameters of the three largest craters on ricochet witness plates with undamaged rear surfaces were measured. In this manner, the diameters and velocities subsequently calculated would represent upper bounds on ricochet debris sizes and speeds. Next, the equations for penetration depth and crater diameter were solved for particle diameter and velocity in terms of all other parameters, such as density, yield strength, wave speed, and so forth. Substitution of the appropriate parameter values in these equations yielded an estimate for the size and speed of the particle that produced a particular crater. This procedure was repeated for each crater using 12 penetration depth equations and 6 crater diameter equations. These equations, some rewritten for consistency, are listed in the Appendix.

Theoretically, this method should have resulted in 72 estimates for the diameter and 72 estimates for the velocity of each crater producing projectile. However, in the process of pairing the penetration depth and crater diameter equations, it became evident that not all equation pairs were compatible. Because of the exponential form of the equations, certain combinations of equations led to powers of zero for an unknown diameter or velocity. These particular equation pairs, therefore, could not be used to solve for the unknown quantities. This situation is analogous to finding the intersection of two parallel lines in Euclidean geometry. Furthermore, even though an equation pair did produce a solution, the resultant particle size occasionally exceeded that of the crater diameter, sometimes by a factor of three or four. However, it was previously shown that the heated material surrounding a high-speed impact crater relaxes as it cools after the impact event, which can cause a reduction in crater diameter and depth of approximately 20–25%.[22,23] Therefore, while it is possible that a crater could have been produced by a particle whose diameter exceeded the size of the crater opening, it is unlikely that the diameter of the particle could have exceeded the surface diameter of the crater it produced by more than 25%. As a result, a particle diameter value greater than 1.25 times a corresponding measured crater surface diameter was rejected. These two considerations reduced the number of calculated values from 72 to approximately 25. The averages of the acceptable diameters and velocities for each particle were then assumed to be valid estimates of its actual diameter and speed.

Measured crater depths and surface diameters are given in Table 1 for the three largest craters; the resulting estimated particle diameters and velocities corresponding to these depths and diameters are presented in Table 2. The average values of the diameters and velocities (plus and minus a standard deviation) are shown in Table 3 as functions of original projectile diameter and impact velocity. The percent differences between

Table 1 Measured penetration depths, crater diameters (p_i, d_{hi} . . . penetration depth, surface diameter of ith crater)

Impact parameters				Penetration depths and diameters, cm					
Test number	Velocity, km/s	θ, deg	d, cm	p_1	d_{h1}	p_2	d_{h2}	p_3	d_{h3}
EHAB	6.91	75	0.795	0.615	0.734	0.368	0.686	0.483	0.566
EHBP	7.22	75	0.635	0.495	0.650	0.361	0.602	0.310	0.445
EHCP	7.58	75	0.475	0.386	0.599	0.318	0.447	0.345	0.422
EHRP2	6.80	65	0.795	0.371	0.632	0.229	0.445	0.211	0.445
EHRP5	7.51	65	0.635	0.305	0.528	0.330	0.546	0.203	0.411
EHRP1	6.87	60	0.795	0.140	0.254	0.094	0.241	0.117	0.244
EHRP4	7.65	60	0.635	0.152	0.279	0.216	0.371	0.157	0.328
EHRP7	7.98	60	0.475	0.323	0.488	0.254	0.396	0.203	0.465
EHRP3	6.78	45	0.795	0.165	0.368	0.150	0.320	0.135	0.343
EHRP6	7.57	45	0.635	0.097	0.201	0.114	0.267	0.084	0.211
EHRP8	7.34	45	0.475	0.155	0.262	0.137	0.279	0.168	0.295

Table 2 Calculated particle diameters and velocities (d_i, V_i . . . average diameter, velocity of particle causing ith crater)

Impact parameters				Particle diameters (cm) and velocities (km/s)					
Test number	Velocity, km/s	θ, deg	d, cm	d_1	V_1	d_2	V_2	d_3	V_3
EHAB	6.91	75	0.795	0.472	2.40	0.452	1.97	0.346	2.45
EHBP	7.22	75	0.635	0.389	2.58	0.395	2.06	0.254	2.50
EHCP	7.58	75	0.475	0.390	2.20	0.253	2.55	0.261	2.47
EHRP2	6.80	65	0.795	0.350	1.96	0.361	2.03	0.243	1.99
EHRP5	7.51	65	0.635	0.302	2.28	0.253	2.25	0.289	1.80
EHRP1	6.87	60	0.795	0.413	1.98	0.289	1.85	0.260	2.21
EHRP4	7.65	60	0.635	0.176	2.08	0.240	2.02	0.208	2.01
EHRP7	7.98	60	0.475	0.125	2.06	0.157	1.97	0.123	1.95
EHRP3	6.78	45	0.795	0.160	2.09	0.140	1.93	0.148	2.19
EHRP6	7.57	45	0.635	0.224	1.98	0.183	2.24	0.191	1.97
EHRP8	7.34	45	0.475	0.169	2.07	0.168	2.13	0.186	2.09

the actual crater depths and surface diameters in Table 1 and those calculated using the equations in the Appendix and the corresponding particle diameters and impact velocities are shown in Table 4. An examination of Tables 1-4 reveals several interesting features.

First, high obliquity impacts and impacts by large projectiles produce larger ricochet debris particles than impacts at low obliquities or impacts by small projectiles (Tables 2 and 3). This is a quantitative verification of the qualitative statement that the severity of the ricochet damage is directly related to the trajectory obliquity and size of the original projectile.

Second, the diameters of the ricochet debris particles are approximately 40% of the parent projectile diameters (Table 2). Since particle volume is proportional to the third power of its diameter, it can also be said that the volume of a ricochet debris particle is typically 6.4% of the parent projectile volume.

Third, ricochet debris particle velocity does not seem to vary significantly with respect to the obliquity and speed of the original projectile but can vary between 24 and 36% of the original impact velocity (Table 3).

Fourth, particle diameters and speeds calculated using this technique will probably yield surface diameters fairly close to the actual values, but will overestimate penetration depths by an average of approximately 20% (Table 4). However, since the average penetration depth error is positive, the error is on the side of safety. The larger penetration depth prediction error is due to the fact that the penetration depth equations used in this study often differ from each other by as much as 30% in their prediction of penetration depth. Predictions of crater diameter, however, more closely approximated the actual values because there were fewer crater diameter equations and because the crater diameter equations generally yielded values that were within 5-10% of each other.

Table 3 Average ricochet particle diameters and velocities as a function of original projectile obliquity and original projectile diameter (original impact velocity $6.7 < V < 8.0$ km/s)

θ, deg	d_{avg} (cm)	V_{avg} (km/s)
45	0.174 ± 0.024	2.07 ± 0.10
60	0.221 ± 0.087	2.01 ± 0.09
65	0.299 ± 0.044	2.05 ± 0.17
75	0.357 ± 0.079	2.35 ± 0.21
d (cm)	d_{avg} (cm)	V_{avg} (km/s)
0.475	0.203 ± 0.080	2.17 ± 0.20
0.635	0.258 ± 0.070	2.15 ± 0.19
0.795	0.303 ± 0.110	2.08 ± 0.18

Design of External Debris Containment Shields

Development of Shield Concept

It has been demonstrated that an obliquely incident hypervelocity projectile will produce ricochet debris particles that can severely damage external flight critical systems of a spacecraft. In the event of an onorbit impact near mission-critical subsystems, the ricochet debris that is produced must be contained in order to guarantee the safety of the mission. Additionally, ricochet debris must be contained to avoid jeopardizing the safety of future missions into the same environment. It is proposed that external spacecraft subsystems can be efficiently protected from ricochet debris impact damage by a series of rectangular panels that are judiciously designed and placed around the exterior of a spacecraft module. The exact placement and distribution of these panels will depend on the orientation of the longitudinal axis with respect to the flight direc-

Table 4 Prediction errors using calculated particle diameters and velocities

Impact parameters				Prediction errors, %					
Test number	Velocity, km/s	θ, deg	d, cm	p_1	d_{h1}	p_2	d_{h2}	p_3	d_{h3}
EHAB	6.91	75	0.795	−6.0	16.7	28.0	5.4	−10.9	12.7
EHBP	7.22	75	0.635	1.8	13.8	17.9	7.8	3.0	6.8
EHCP	7.58	75	0.475	15.1	11.9	1.7	7.1	−6.2	14.6
EHRP2	6.80	65	0.795	19.0	6.2	16.3	7.7	24.2	−13.7
EHRP5	7.51	65	0.635	9.3	9.0	14.5	11.3	43.3	−14.8
EHRP1	6.87	60	0.795	16.5	4.8	24.1	−0.4	39.5	−8.7
EHRP4	7.65	60	0.635	24.1	4.5	17.4	5.4	38.5	−6.4
EHRP7	7.98	60	0.475	37.0	−7.0	40.2	−14.2	47.7	−16.1
EHRP3	6.78	45	0.795	23.1	4.6	50.1	−16.6	41.2	−5.6
EHRP6	7.57	45	0.635	40.2	−11.5	39.1	−9.8	45.4	−19.2
EHRP8	7.34	45	0.475	16.5	6.6	33.6	−8.3	19.6	4.9

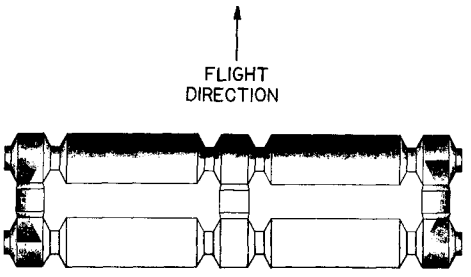

Fig. 2 Assumed space station module orientation and flight

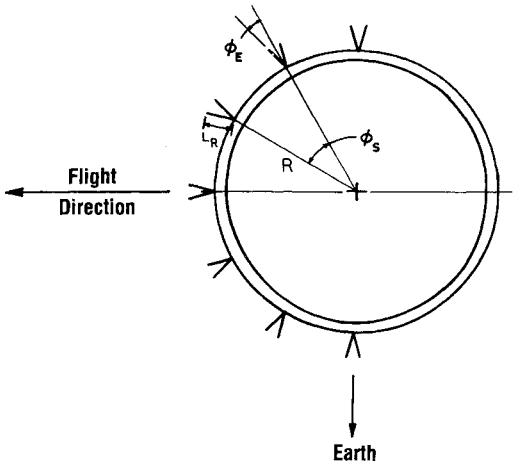

Fig. 3 Space station module cross section with protection panel parameters.

tion vector and on several phenomenological considerations that are discussed below.

Although the concepts and procedures developed in the following paragraphs are applicable to any type of spacecraft geometry and orientation, for the purposes of this investigation, it is assumed that the spacecraft for which the external protective system is to be designed is cylindrical and is oriented such that its velocity vector is perpendicular to its longitudinal axis. In the case of the Space Station Freedom, this assumption implies that the station modules would be configured as shown in Fig. 2. In this arrangement, the shaded areas in the figure are those that are most likely to be impacted by orbital debris. Although only the containment of ricochet particles formed by space debris impact will be addressed in the following paragraphs, the equations that are developed can be applied to the problem of meteoroid impact as well.

In this module orientation, the proposed panels would run parallel to the longitudinal axis of the modules and would be evenly spaced along its circumference. If the space station were rotated so that its flight direction vector were parallel to its longitudinal axis, the shield panels would run perpendicular to and would be evenly spaced along its longitudinal axis. A cross section of a typical module showing the module wall, bumper plate, and an array of containment shield elements is given in Fig. 3. A V-shaped panel arrangement was chosen as the basic protection unit because each panel of the protection unit will serve as a bumper for the other panel and will trap any secondary "penetration" debris that may form as a result of a ricochet debris particle impact. Naturally, depending on the location of mission-critical subsystems, some shields may be eliminated or added to achieve a desired protection level.

In the design of such a containment shield system, it is assumed that the radius R of the spacecraft is a known quantity. The unknown quantities that need to be determined are the element panel length L_r, panel thickness t_p, panel inclination ϕ_e, and the element separation ϕ_s. Acceptable design values for these parameters are limited by the following phenomenological considerations.

1) The most dangerous ricochet debris particles are formed by impacts whose trajectory obliquities are greater than 60 deg.[2] Therefore, it is required that the angular separation of the containment shield elements be such that any projectile impacting the spacecraft between two adjacent shield elements have a trajectory obliquity of no more than 60 deg (design condition 1).

2) Low obliquity impacts produce ricochet debris particles that can travel along trajectories of 30 deg with respect to the plane of the bumper plate. These trajectory obliquities decrease as the obliquity of the parent projectile increases.[2] Therefore, it is required that the length L_r of each containment shield element panel be sufficient to trap ricochet debris formed from an impact with a low trajectory obliquity, i.e., less than 45 deg (design condition 2).

The design procedure will basically consist of selecting a panel length, panel inclination, and an element separation and then ensuring that the chosen values satisfy design conditions 1 and 2. Panel thickness is calculated using a technique currently employed in the design of dual-wall structures.[24]

Design Equations

Consider a projectile about to strike the external bumper wall of a cylindrical spacecraft with radius R (Fig. 4). In the following paragraphs, the terms "downstream" and "upstream" refer, respectively, to the shield elements in front of and behind an actual or projected impact site. Let ϕ_m be the angular separation between the site of impact and a downstream shielding element, γ the obliquity of its trajectory with respect to the outward normal of the spacecraft hull, and let γ_{max} be the maximum value of all such obliquities. The maximum obliquity occurs when the trajectory of an incoming projectile grazes an upstream shield element and terminates at

the base of an adjacent downstream element. Thus, when $\gamma = \gamma_{max}$, then $\phi_m = 0$.

According to design condition 1, the shield elements must be spaced so that all trajectory obliquities are less than 60 deg. In Fig. 5, a projectile traveling along a trajectory with an obliquity γ grazes the outermost point D of shield element panel DE and impacts at point A; point C lies at the foot of the perpendicular drawn from point D to the extension of radius EF; and point B is the foot of the perpendicular from point C to the extension of radius AF. Then angle $CFB = \phi_s - \phi_m$, angle $CED = \phi_e$, and angle $DAB = \gamma$. Let angle $ECA = \alpha$, angle $CDA = \epsilon$, and angle $CAB = \gamma_0$; then angle $CAD = \gamma_0 - \gamma$. Last, let $CA = z$, $DA = u$, $CE = v$, $CB = y$, and $BA = x$. In triangle FBC,

$$x = (R + L_r \cos\phi_e)\cos(\phi_s - \phi_m) - R \tag{1}$$

$$y = (R + L_r \cos\phi_e)\sin(\phi_s - \phi_m) \tag{2}$$

$$\gamma_0 = \tan^{-1}(y/x) \tag{3}$$

$$z = (x^2 + y^2)^{1/2} \tag{4}$$

In triangle DCE,

$$w = L_r \sin\phi_e \tag{5a}$$

$$v = L_r \cos\phi_e \tag{5b}$$

Applying the law of cosines to triangle DCA yields

$$w^2 = u^2 + z^2 - 2uz\cos(\gamma_0 - \gamma) \tag{6}$$

while applying the law of sines to triangle CAD yields

$$\frac{z}{\sin\epsilon} = \frac{u}{\sin(90 - \alpha)} \tag{7}$$

In triangle ACF,

$$\alpha = \gamma_0 - (\phi_s - \phi_m) \tag{8}$$

and in triangle CAD,

$$\epsilon = 90 + \gamma - (\phi_s - \phi_m) \tag{9}$$

Substituting Eqs. (8) and (9) into Eq. (7) yields

$$u = gz \tag{10}$$

where

$$g = \cos\left[\gamma_0 - (\phi_s - \phi_m)\right] / \cos\left[\gamma - (\phi_s - \phi_m)\right] \tag{11}$$

Substituting Eq. (10) into Eq. (6) and combining Eqs. (5a) and (6) yields

$$g^2 z^2 + z^2 - 2gz^2\cos(\gamma_0 - \gamma) = L_r^2 \sin^2\phi_e \tag{12}$$

Substituting for z according to Eq. (4) yields

$$g^2 - 2g\cos(\gamma_0 - \gamma) + 1 - L_r^2 \sin^2\phi_e \Big/ \Big[R^2 + (R + L_r\cos\phi_e)^2 - 2R(R + L_r\cos\phi_e)\cos(\phi_s - \phi_m)\Big] = 0 \tag{13}$$

where $g(\gamma, \phi_0, \phi_s, \phi_m)$ is given by Eq. (11) and

$$\gamma_0 = \tan^{-1}\left\{(R + L_r\cos\phi_e)\sin(\phi_s - \phi_m) \Big/ \left\{L_r\cos\phi_e - (R + L_r\cos\phi_e)\left[1 - \cos(\phi_s - \phi_m)\right]\right\}\right\} \tag{14}$$

From Fig. 4, $\gamma = \gamma_{max}$ when $\phi_m = 0$. To calculate γ_{max}, set

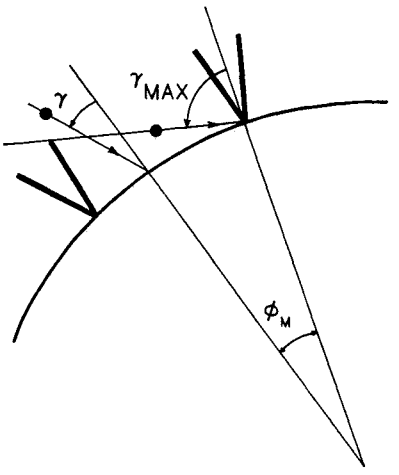

Fig. 4 Space debris trajectories.

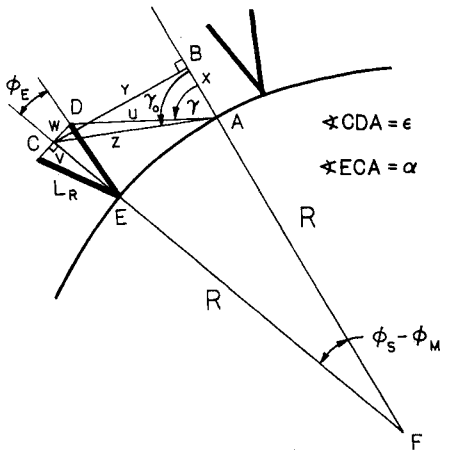

Fig. 5 Protection panel geometry for design condition 1.

$\phi_m = 0$ in Eq. (13) and solve for γ. If $\gamma = \gamma_{max} < 60$ deg for the chosen values of L_r and ϕ_e, then design condition 1 is satisfied.

According to design condition 2, shield element panels must be long enough to contain ricochet debris formed by low obliquity impacts. Panel length varies directly with the distance from the impact site to the foot of the panel. Maximum panel length will be achieved by considering a low obliquity impact trajectory that grazes the outermost point of an upstream element panel and places the impact site as far away as possible from the adjacent downstream element.

In Fig. 6, point A is the point of impact on the bumper of a projectile traveling along such a trajectory; BD is the downstream shield element panel that must be long enough to contain the ricochet debris within angle BAD; point C lies at the intersection of line AD and the extension of radius BF; point G is a point on the line tangent to the circle at point A; point H is a point on the extension of radius AF. Then angle $AFC = \phi_m$, angle $CBD = \phi_e$, angle $CAG = 30$ deg, angle $CAF = 120$ deg, angle $ACF = 60$ deg $- \phi_m$, $AF = BF = R$, and $BD = L_r$. Let the trajectory obliquity (angle EAH) be equal to 30 deg, and let $CB = u$. Applying the law of sines to triangle CAF yields

$$\frac{u + R}{\sin 120} = \frac{R}{\sin(60 - \phi_m)} \tag{15}$$

Solving for u yields

$$u = R\left[1 - (\cos\phi_m - 0.577\sin\phi_m)\right] / (\cos\phi_m - 0.577\sin\phi_m) \tag{16}$$

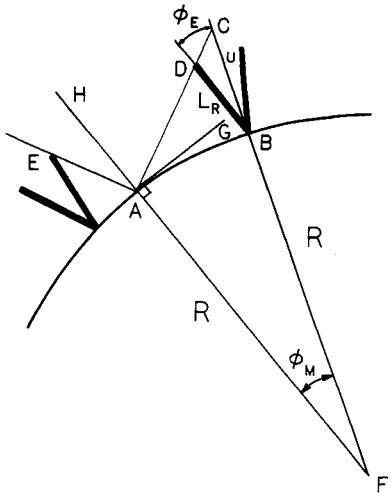

Fig. 6 Protection panel geometry for design condition 2.

Applying the law of sines to triangle CBD yields

$$\frac{u}{\sin(120+\phi_m-\phi_e)} = \frac{L_r}{\sin(60-\phi_m)} \tag{17}$$

Solving for L_r yields

$$L_r = R\left[1-f(\phi_m, 0)\right]/f(\phi_m,\phi_e) \tag{18}$$

where

$$f(x,y) = \cos(x-y) - 0.577\sin(x-y) \tag{19}$$

Thus, if the value of L_r for the downstream panel calculated using Eq. (18) is less than the assumed value of L_r, then the assumed panel length is sufficient and design condition 2 is satisfied.

Panel thicknesses can be calculated using a modified form of the following equation for rear-sheet thickness of a dual-wall structure[24]

$$t_2/d = 5.08\,V^{0.278}(t_1/d)^{-0.528}(h/d)^{-1.39} \tag{20}$$

where t_1 and t_2 are the thicknesses of the first and second sheets, respectively, and h is the separation between the two sheets. Since the two panels are not uniformly spaced, an equivalent "separation distance" was calculated as follows. Based on previous examinations of damaged ricochet witness plates, it was assumed that the majority of ricochet particle impacts will occur within a distance of $L_r/2$ away from the base of the shield element. Using the relationship between arc length, angle, and radius, the separation distance was approximated by the following equation.

$$h \simeq (L_r/2)(2\phi_e) = L_r\phi_e \tag{21}$$

To equally protect against impacts above and below the flight direction vector, the element design is assumed to be symmetric with respect to the outward normal of the spacecraft. Therefore, letting $t_1 = t_2 = t_p$, substituting for h in Eq. (20) according to Eq. (21), and solving for t_p yields the following expression for panel thickness.

$$t_p/d = 2.897\,V^{0.182}(L_r\phi_e/d)^{-0.910} \tag{22}$$

Design Procedure

The procedure to be used for the design of containment shielding panels is as follows.

Step 1

Input assumed values for ϕ_s, ϕ_e, L_r, and R. Satisfactory initial values for these parameters are $\phi_s = 10$ deg, $\phi_e = 5$ deg, and $L_r = 0.1$–0.2 R.

Table 5 Panel length (cm) and thickness (cm) as a function of panel inclination and shield element separation

	Panel inclination, ϕ_e							
	5 deg		10 deg		15 deg		20 deg	
ϕ_s	L_r	t_p	L_r	t_p	L_r	t_p	L_r	t_p
5 deg	12.19	0.222	11.58	0.124	10.97	0.090	10.67	0.071
10 deg	27.43	0.106	25.91	0.060	24.38	0.044	23.47	0.035
15 deg	48.77	0.063	44.20	0.037	42.67	0.026	38.10	0.023
20 deg	73.15	0.043	67.06	0.025	60.96	0.019	56.38	0.016

Step 2

Calculate γ_{max} using Eq. (13) with $\phi_m = 0$. Is $\gamma_{max} < 60$ deg?

If yes, proceed to step 3; if no, choose a smaller ϕ_s or a larger L_r and repeat this step.

Step 3

Calculate ϕ_m for the assumed values of ϕ_s, ϕ_e, and L_r using Eq. (13) with $\gamma = 30$ deg.

Step 4

Calculate the length L_r of the downstream shielding element panel using Eq. (18). Is the assumed length L_r greater than the downstream length L_r? If yes, proceed to step 5; if no, choose a larger L_r or a smaller ϕ_s and go to step 2.

Step 5

The values of ϕ_s, ϕ_e, and L_r are acceptable. Calculate t_p using Eq. (22).

Several examples of panel design using this procedure and the accompanying equations are presented in the next section.

Examples

A matrix of acceptable design values for ϕ_s, ϕ_e, L_r, and t_p is given in Table 5. Panel length values were obtained for a spacecraft radius of 2.235 m; thickness values were obtained using an average value for ricochet particle diameter and speed, namely, $d = 0.25$ cm and $V = 2.1$ km/s. It can be seen in Table 5 that a small change in ϕ_e produces only a minor change in L_r whereas a similar small change in ϕ_s results in a major change in L_r. However, panel thickness is seen to be strongly dependent on the angle of inclination as well as the separation angle.

Conclusions and Recommendations

An efficient protection mechanism that will safeguard external spacecraft systems against ricochet debris impact damage and that will also contain the spread of ricochet debris particles has been developed. The mechanism consists of a series of rectangular panels that are arranged in V-shaped units and distributed along the exterior of a spacecraft compartment or module. Panel dimensions were found to be strongly dependent on the external spatial distribution of the protection units and on the inclination of the panels with respect to the outwardly pointing normal of the spacecraft module at each unit location. High obliquity impacts were observed to have a very high potential for damage to external spacecraft systems because of the extremely large volume of ricochet debris particles that they produce. An analysis of ricochet witness plate crater damage revealed that an average ricochet debris particle diameter can be as large as 40% of the parent projectile diameter and can travel at a speed of up to 36% of the original impact velocity. It is imperative that the issue of ricochet debris impact damage to external spacecraft systems be addressed in the

design of spacecraft that are developed for the meteoroid or space debris environment.

Appendix

Penetration Depth Equations

Reference 25:

$$p/d = 2.28(\rho_p/\rho_t)^{1/3}(V/C)^{2/3}, \qquad V < 9 \text{ km/s} \qquad \text{(A1)}$$

Reference 26:

$$p/d = 1.96(\rho_p/\rho_t)^{1/2}(V/C)^{2/3}, \qquad V < 6 \text{ km/s} \qquad \text{(A2)}$$

Reference 27:

$$p/d = 1.5(\rho_p/\rho_t)^{1/3}(\rho_p V^2/2S_t)^{1/3}, \qquad V < 8 \text{ km/s} \qquad \text{(A3)}$$

Reference 28:

$$p/d = 2.35(\rho_p/\rho_t)^{0.70}(V/C)^{2/3}, \qquad V < 9 \text{ km/s} \qquad \text{(A4)}$$

Reference 29:

$$p/d = 0.63(\rho_p V^2/\sigma_{yt})^{1/3}, \qquad V < 7 \text{ km/s} \qquad \text{(A5)}$$

Reference 30:

$$p/d = 0.482(\rho_p/\rho_t)^{0.537}(V/C)^{0.576}(Y_t/\rho_t C^2)^{-0.235}, \qquad V < 21 \text{ km/s} \qquad \text{(A6)}$$

Reference 31:

$$p/d = 8.355 \times 10^{-4}\rho_p^{2/3}\rho_t^{-1/3}(V^2/H_t)^{1/3}, \qquad V < 9.5 \text{ km/s} \qquad \text{(A7)}$$

Reference 32:

$$p/d = 2.0(\rho_p/\rho_t)^{4.52}(V/C)^{1.136}, \qquad V < 9 \text{ km/s} \qquad \text{(A8)}$$

Reference 33:

$$p/d = 0.311(\rho_p/\rho_t)^{0.17}(\rho_p V^2/S_t)^{0.285}, \qquad V < 7 \text{ km/s} \qquad \text{(A9)}$$

Reference 34:

$$p/d = 0.36(\rho_p/\rho_t)^{2/3}(\rho_p V^2/B_t)^{1/3}, \qquad V < 6 \text{ km/s} \qquad \text{(A10)}$$

Reference 35:

$$p = 2.973 \times 10^{-7} d^{1.1} H_t^{-0.25} \rho_p^{0.5} \rho_t^{-0.167} V^{4/3}, \qquad V < \simeq 3 \text{ km/s} \qquad \text{(A11)}$$

$$p = 1.129 \times 10^{-6} d^{1.056} H_t^{-0.25} \rho_p^{0.5} \rho_t^{-0.167} E_t^{-0.33} V^{4/3}, \qquad V < \simeq 3 \text{ km/s} \qquad \text{(A12)}$$

Crater Diameter Equations

Reference 36:

$$\alpha d_h^2 p/d^3 = 34(\rho_p/\rho_t)^{3/2}(V/C)^2, \qquad V < 4 \text{ km/s} \qquad \text{(A13)}$$

Reference 33:

$$\alpha d_h^2 p/d^3 = 0.120(\rho_p/\rho_t)^{0.5}(\rho_p V^2/S_t)^{0.845}, \qquad V < 7 \text{ km/s} \qquad \text{(A14)}$$

Reference 26:

$$\alpha d_h^2 p/d^3 = 30.25(\rho_p/\rho_t)^{3/2}(V/C)^2, \qquad V < 6 \text{ km/s} \qquad \text{(A15)}$$

Reference 28:

$$\alpha d_h^2 p/d^3 = 44.10(\rho_p/\rho_t)^{2/3}(V/C)^2, \qquad V < 9 \text{ km/s} \qquad \text{(A16)}$$

Reference 31:

$$\alpha d_h^2 p/d^3 = 2.65 \times 10^{-9}\rho_p^{7/6}\rho_t^{-1/2}V^2/H_t, \qquad V < 9.5 \text{ km/s} \qquad \text{(A17)}$$

Reference 34:

$$\alpha d_h^2 p/d^3 = 0.16(\rho_p/\rho_t)^{3/2}\rho_p V^2/B_t, \qquad V < 6 \text{ km/s} \qquad \text{(A18)}$$

Notation

d_h = crater surface diameter, cm
d = projectile diameter, cm
p = crater depth, cm
B_t = target material Brinell hardness, dynes/cm^2
C = speed of sound in target material, cm/s
E_t = target material elastic modulus, GPa
H_t = target material Brinell hardness number, kg/mm^2
S = target material static shear strength, dynes/cm^2
S_t = target material dynamic hardness, dynes/cm^2
Y_t = target material dynamic shear strength, dynes/cm^2
V = projectile impact velocity
α = crater shape factor; = 0.75 if $p > d_h/2$, = 1.00 if $p \le d_h/2$
ρ_p = projectile material mass density, gm/cm^3
ρ_t = target material mass density, gm/cm^3
σ_{yt} = target material dynamic yield strength, dynes/cm^2

Material Properties

$B_t = 1.27 \times 10^{10}$ dynes/cm^2
$C = 5.10 \times 10^5$ cm/s
$E_t = 7.38 \times 10^{10}$ N/m^2
$S = 2.83 \times 10^9$ dynes/cm^2
$S_t = 6.37 \times 10^{10}$ dynes/cm^2
$Y_t = 2.78 \times 10^9$ dynes/cm^2
$\rho_p = 2.71$ gm/cm^3
$\rho_t = 2.84$ gm/cm^3
$\sigma_{yt} = 1.85 \times 10^{10}$ dynes/cm^2
$H_t = 130$ kg/mm^2

Acknowledgments

The authors wish to acknowledge the support of the National Aeronautics and Space Administration/American Society of Engineering Education Summer Faculty Fellowship Program along with Michael Freeman, the University of Alabama Director, and Ernestine Cothran, the Marshall Space Flight Center Program Codirector. The authors wish to express their appreciation to Raymond Gause, Chief of the Engineering Physics Division, for his suggestions in the development of the ricochet debris containment shield system, and to Hubert Smith of the Laboratory Support Branch for conducting the impact testing that made this report possible.

References

[1]Coronado, A. R., Gibbins, M. N., Wright, M. A., and Stern, P. H., *Space Station Integrated Wall Design and Penetration Damage Control,* Boeing Aerospace Co., Seattle, WA, D180-30550-1, Contract NAS8-36426, 1987.

[2]Schonberg, W. P., and Taylor, R. A., "Penetration and Ricochet Phenomena in Oblique Hypervelocity Impact," *AIAA Journal,* Vol. 27, No. 5, 1989, pp. 639-646.

[3]Whipple, E. L., "Meteorites and Space Travel," *Astronomical Journal,* Vol. 52, March 1947, p. 137.

[4]Burch, G. T., "Multi-plate Damage Study," Air Force Armament Laboratory, Eglin AFB, FL, AF-ATL-TR-67-116, 1967.

[5]D'Anna, P. J., "A Combined System Concept for Control of the Meteoroid Hazard to Space Vehicles," *Journal of Spacecraft,* Vol. 2, No. 1, 1965, pp. 33-37.

[6]Lundeberg, J. F., Lee, D. H., and Burch, G. T., "Impact Penetration of Manned Spacecraft," *Journal of Spacecraft,* Vol. 3, No. 2, 1966, pp. 182-187.

[7]Lundeberg, J. F., Stern, P. H., and Bristow, R. J., "Meteoroid Protection for Spacecraft Structures," NASA CR 54201, 1965.

[8]McMillan, A. R., "Experimental Investigations of Simulated Meteoroid Damage to Various Spacecraft Structures, NASA CR 915, 1968.

[9]Maiden, C. J., Gehring, J. W., and McMillan, A. R., "Investigation of Fundamental Mechanism of Damage to Thin Targets by Hypervelocity Projectiles," General Motors Defense Lab., Santa Barbara, CA, GM-DRL-TR-63-225, 1963.

[10]Maiden, C. J., and McMillan, A. R., "An Investigation of the Protection Afforded a Spacecraft by a Thin Shield," *AIAA Journal,* Vol. 2, No. 11, 1964, pp. 1992–1998.

[11]Nysmith, C. R., "Penetration Resistance of Double Sheet Structures at Velocities to 8.8 km/sec," NASA TN D-4568, 1968.

[12]Riney, T. D., and Halda, E. J., "Effectiveness of Meteoroid Bumpers Composed of Two Layers of Distinct Materials," *AIAA Journal,* Vol. 6, No. 2, 1968, pp. 338–344.

[13]Swift, H. F., Bamford, R., and Chen, R., "Designing Space Vehicle Shields for Meteoroid Protection: A New Analysis," *Advances in Space Research,* Vol. 2, Dec. 1983, pp. 219–234.

[14]Wallace, R. R., Vinson, J. R., and Kornhauser, M., "Effects of Hypervelocity Particles on Shielded Structures," *ARS Journal,* Aug. 1962, pp. 1231–1237.

[15]Wilkinson, J. P. D., "A Penetration Criterion for Double-Walled Structures Subject to Meteoroid Impact," *AIAA Journal,* Vol. 7, No. 10, 1968, pp. 1937–1943.

[16]Taylor, R. A., "A Space Debris Simulation Facility for Spacecraft Materials Evaluation," *SAMPE Quarterly,* Vol. 18, Feb. 1987, pp. 28–34.

[17]Schonberg, W. P., " Hypervelocity Impact Penetration Phenomena in Aluminum Space Structures," *Journal of Aerospace Engineering,* (to be published).

[18]Kessler, D. J., "Orbital Environment for Space Station," JSC20001.

[19]Schonberg, W. P., Taylor, R. A, and Horn, R. A, "An Analysis of Penetration and Ricochet Phenomena in Oblique Hypervelocity Impact," NASA TM-100319, 1988.

[21]Schonberg, W. P., and Taylor, R. A., "Analysis of Oblique Hypervelocity Impact Phenomena for Meteoroid/Space Debris Protection System Design," *Proceedings of the AIAA SDM Issues of the International Space Station Symposium,* AIAA, Washington, DC, 1988; also AIAA Paper 88-2463, 1988, pp. 72–81.

[22]Rolsten, R. F., and Hunt, H. H., "Impact Force and Crater Surface Area," *AIAA Journal,* Vol. 1, No. 8, 1963, pp. 1893–1895.

[23]Rolsten, R. F., and Hunt, H. H., "Impact Force per Crater Area Related to Tensile Strength," *Journal of Spacecraft and Rockets,* Vol. 1, No. 3, 1964, pp. 351–352.

[24]Nysmith, C. R., "An Experimental Impact Investigation of Aluminum Double-Sheet Structures," *Proceedings of the AIAA Hypervelocity Impact Conference,* AIAA, New York, 1969; also AIAA Paper 69-375, 1969.

[25]Sawle, D. R., "Hypervelocity Impact in Thin Sheets and Semi-Infinite Targets at 15 km/sec," *AIAA Journal,* Vol. 8, No. 7, 1970, pp. 1240–1244.

[26]Bruce, E. P., "Review and Analysis of High Velocity Impact Data," *Proceedings of the Fifth Hypervelocity Impact Symposium,* 1962, pp. 439–474.

[27]Schneider, E., "Velocity Dependence of Some Impact Phenomena," *Proceedings of the Comet Halley Micrometeoroid Hazard Workshop,* ESA SP-153, ESA Scientific and Technical Publications Branch, The Netherlands, 1979, pp. 101–107.

[28]Goodman, E. H., and Liles, C. D., "Particle-Solid Impact Phenomena," *Proceedings of the Sixth Hypervelocity Impact Symposium,* 1963, pp. 543–577.

[29]Dunn, W. P., "On Material Strengths of the Hypervelocity Impact Problem," *AIAA Journal,* Vol. 4, No. 3, 1966, pp. 535–536.

[30]Sedgwick, R. T., Hageman, L. J., Herrmann, R. G., and Waddell, J. L., "Numerical Investigations in Penetration Mechanics," *International Journal of Engineering Sciences,* Vol. 16, 1978, pp. 859–869.

[31]Christman, D. R., "Target Strength and Hypervelocity Impact," *AIAA Journal,* Vol. 4, No. 10, 1966, pp. 1872–1874.

[32]Summers, J. L., and Charters, A. C., "High-Speed Impact of Metal Projectiles in Targets of Various Materials," *Proceedings of the Third Hypervelocity Impact Symposium,* 1959, pp. 101–113.

[33]Sorenson, N. R., "Systematic Investigation of Crater Formation in Metals," *Proceedings of the Fifth Hypervelocity Impact Symposium,* 1962, pp, 281–325.

[34]Herrmann, W., and Jones, A. H., "Correlation of Hypervelocity Impact Data," *Proceedings of the Fifth Hypervelocity Impact Symposium,* 1962, pp, 389–438.

[35]Cour-Palais, B. G., "Hypervelocity Impact Investigations and Meteoroid Shielding Experience Related to Apollo and Skylab," *Orbital Debris,* NASA CP-2360, 1982, pp. 247–275.

[36]Summers, J. L., "Investigation of High Speed Impact: Regions of Impact and Impact at Oblique Angles," NASA TN D-94, 1959.

Paul F. Mizera
Associate Editor